Inorg. Chem. **2003**, *42*, 365–376

Spectroscopic Studies of the Effect of Ligand Donor Strength on the Fe–NO Bond in Intradiol Dioxygenases

Erik C. Wasinger,[†,||] Mindy I. Davis,[†,||] Monita Y. M. Pau,[†] Allen M. Orville,[§,⊥] Jeffrey M. Zaleski,[†] Britt Hedman,*[,‡] John D. Lipscomb,*[,§] Keith O. Hodgson,*[,†,‡] and Edward I. Solomon*[,†]

Department of Chemistry and Stanford Synchrotron Radiation Laboratory, Stanford University, Stanford, California 94305, and Department of Biochemistry, Molecular Biology and Biophysics and the Center for Metals in Biocatalysis, University of Minnesota, Minneapolis, Minnesota 55455

Received July 26, 2002

The geometric and electronic structure of NO bound to reduced protocatechuate 3,4-dioxygenase and its substrate (3,4-dihydroxybenzoate, PCA) complex have been examined by X-ray absorption (XAS), UV–vis absorption (Abs), magnetic circular dichroism (MCD), and variable temperature variable field (VTVH) MCD spectroscopies. The results are compared to those previously published on model complexes described as $\{FeNO\}^7$ systems in which an $S = {}^5/_2$ ferric center is antiferromagnetically coupled to an $S = 1$ NO^-. XAS pre-edge analysis indicates that the Fe–NO units in $Fe^{III}PCD\{NO^-\}$ and $Fe^{III}PCD\{PCA,NO^-\}$ lack the greatly increased pre-edge intensity representative of most $\{FeNO\}^7$ model sites. Furthermore, from extended X-ray absorption fine structure (EXAFS) analysis, the $Fe^{III}PCD\{NO^-\}$ and $Fe^{III}PCD\{PCA,NO^-\}$ active sites are shown to have an Fe–NO distance of at least 1.91 Å, ≈0.2 Å greater than those found in the model complexes. The weakened Fe–NO bond is consistent with the overall lengthening of the bond lengths and the fact that VTVH MCD data show that $NO^- \rightarrow Fe^{III}$ CT transitions are no longer polarized along the *z*-axis of the zero-field splitting tensor. The weaker Fe–NO bond derives from the strong donor interaction of the endogenous phenolate and substrate catecholate ligands, which is observed from the increased intensity in the CT region relative to that of $\{FeNO\}^7$ model complexes, and from the shift in XAS edge position to lower energy. As NO is an analogue of O_2, the effect of endogenous ligand donor strength on the Fe–NO bond has important implications with respect to O_2 activation by non-heme iron enzymes.

Introduction

The intra- and extradiol dioxygenases are members of the class of mononuclear non-heme iron enzymes that catalyze a variety of important biological reactions involving O_2. The bacterial dioxygenases are fundamental to the aerobic biodegradation of nearly all naturally occurring and man-made aromatic compounds.[1−3] Catechol dioxygenases catalyze the reaction of dioxygen with the aromatic ring of the substrate, leading to rupture of the O−O bond with concomitant insertion of both atoms into the substrate, resulting in ring cleavage. Catechol dioxygenases can be grouped into the intra- and extradiol dioxygenases depending on the position of ring cleavage. For the intradiol dioxygenases, binding of substrate to their high-spin ferric active site activates the substrate for direct attack by dioxygen and cleavage between the hydroxylated carbons, leading to *cis,cis*-muconic acids.[3−5] In contrast, for the extradiol dioxyge-

* Authors to whom correspondence should be addressed. E-mail: Edward.Solomon@stanford.edu. Tel: (650)723-9104. Fax: (650)725-0259 (E.I.S.). E-mail: Hodgson@ssrl.slac.stanford.edu. Tel: (650)926-3153. Fax: (650)926-4100 (K.O.H.). E-mail: lipsc001@tc.umn.edu. Tel: (612)-625-6454. Fax: (612)624-5121 (J.D.L.). E-mail: hedman@ssrl.slac.stanford.edu. Tel: (650)926-3052. Fax: (650)926-4100.

† Department of Chemistry, Stanford University.

‡ Stanford Synchrotron Radiation Laboratory, Stanford University.

§ University of Minnesota.

|| These authors contributed equally to the work.

⊥ Current address: School of Chemistry and Biochemistry, Georgia Institute of Technology, Atlanta, GA 30332.

(1) Dagley, S. In *The Bacteria*; Sokatch, J. R., Ornston, L. N., Eds.; Academic Press: Orlando, 1986; Vol. 10, Chapter 10, pp 527−555.

(2) Levin, M. A.; Gealt, M. A. In *Biotreatment of Industrial and Hazardous Waste*; Levin, M. A., Gealt, M. A., Eds.; McGraw-Hill: New York, 1993; pp 5−7.

(3) Lipscomb, J. D.; Orville, A. M. In *Degradation of Environmental Pollutants by Microorganisms and Their Metalloenzymes*; Sigel, H., Sigel, A., Eds.; Metal Ions in Biological Systems; Marcel Dekker: New York, 1992; Vol. 28, pp 243−298.

(4) Que, L., Jr.; Ho, R. Y. N. *Chem. Rev.* **1996**, *96*, 2607−2624.

(5) Solomon, E. I.; Brunold, T.; Davis, M. I.; Kemsley, J. N.; Lee, S.-K.; Lehnert, N.; Neese, F.; Skulan, A. J.; Yang, Y.-S.; Zhou, J. *Chem. Rev.* **2000**, *100*, 235−349.

10.1021/ic025906f CCC: $25.00
Published on Web 12/17/2002

Scheme 1. Substrate Binding to PCD{}[a]

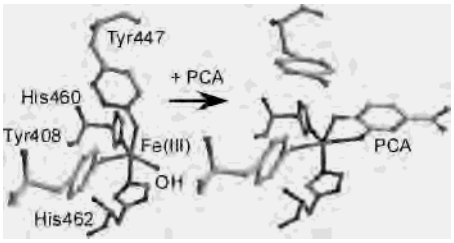

[a] Reprinted with permission from ref 16. Copyright 2002 American Chemical Society.

nases, substrate binding activates a ferrous center for dioxygen reactivity and cleavage of the substrate ring on the distal or proximal side of the hydroxyl groups, leading to muconic semialdehydes.[3−5]

Protocatechuate 3,4-dioxygenase (PCD, EC 1.13.11.3) catalyzes the cleavage of protocatechuate (PCA) to β-carboxy-*cis,cis*-muconate with the incorporation of both atoms from molecular oxygen.[6] X-ray crystallography has been useful in providing information about the resting, substrate-bound, and inhibitor-bound forms of PCD from *Pseudomonas putida* and *Acinetobacter calcoaceticus* ADP1.[7−13] The resting ferric site (Fe^{III}PCD{}) is trigonal bipyramidal with axial tyrosinate (Tyr447) and histidine ligands (His462) and equatorial histidine (His460), tyrosinate (Tyr408), and a water-based ligand, which was shown by X-ray absorption spectroscopy (XAS) to be a hydroxide (Scheme 1).[14,15] A detailed spectroscopic study revealed that the two tyrosinates are inequivalent, with the equatorial tyrosinate adopting a smaller $Fe-O-C_{tyr}$ bond angle and hence a stronger bond to the Fe^{III} than the axial tyrosinate.[16] Upon substrate binding this axial tyrosinate as well as the hydroxide dissociate, which may facilitate the deprotonation of the substrate during the binding process. The substrate-bound form (Fe^{III}PCD{PCA}) is square pyramidal with His460, the equatorial histidine of the resting site, at the apical position (Scheme 1). The equatorial tyrosinate, which has a strong bonding interaction with the iron, is believed to help lead to the asymmetric binding of substrate, with the Fe−O bond trans to Tyr408 being lengthened.[10] The open position is believed to be the binding site for the distal oxygen atom in the peroxy-substrate intermediate during catalysis, thereby facilitating O−O bond cleavage.[3,10] Consequently, it is of mechanistic importance to understand the properties of small molecule binding to the iron center.

While an oxygen intermediate has been observed by stopped flow for PCD,[9,17] currently the amount that can be produced is not sufficient for detailed spectroscopic studies. Alternatively, NO has been used as a dioxygen analogue. In the class of mononuclear non-heme iron enzymes,[5] NO binding to a ferrous center usually leads to an {FeNO}^{7} system (where 7 indicates the sum of the d and NO π^* electrons), which has an $S = {}^3/_2$ spin state.[18,19] This is described as an $S = {}^5/_2$ ferric center antiferromagnetically coupled to an $S = 1$ NO^-, discussed in detail elsewhere.[20] Fe^{III}PCD{} does not bind NO in its native ferric form; upon reduction, however, the ferrous center (Fe^{II}PCD{}) binds NO to form an $S = {}^3/_2$ PCD{FeNO}^{7} species,[21] which from ref 20 is referred to in this study as Fe^{III}PCD{NO^-}. For these $D > 0$, $S = {}^3/_2$ systems, the splitting of the $g_\perp = 4$ resonances is very sensitive to the *E/D* ratio. EPR studies showed that the species formed were quite different ($E/D = 0.055$ and $E/D = 0.175$, respectively).[21,22] While there is not yet a crystal structure of NO bound to PCD, there are crystal structures of high-spin oxidized PCD^{III}{INO,CN^-} and PCD^{III}{NNO,CN^-} where INO (2-hydroxyisonicotinic acid *N*-oxide) or NNO (6-hydroxynicotinic acid *N*-oxide) are substrate analogues that mimic the proposed ketonization of the substrate.[10] These structures are interesting because the Fe−CN angle is bent to 145° due to hydrogen bonding of the CN^- ligand with the amide nitrogen of Tyr16. Similar interactions would presumably also be important in orienting the bond to both NO^- and dioxygen and thus the structures provide a reasonable approximation for the geometry of the Fe^{III}PCD{PCA,NO^-} species.

Several model complexes also have the $S = {}^3/_2$ spin state and can be used to gain insight into NO binding to the enzymes, in particular, $[Fe(EDTA)NO]^{2-}$,[18,20,23−25] $[Fe(tpa)ClNO]^+$,[26] $[Fe(Me_3TACN)(NO)(N_3)_2]$,[20] and [Fe(tris(*N*-R-carbamoylmethyl)amine^{i}Pr)(NO)]$^-$.[27] Brown et al. have

(6) Fujisawa, H.; Hayaishi, O. *J. Biol. Chem.* **1968**, *243*, 2673−2681.
(7) The CD spectra of PCD{} isolated from *P. putida* and *B. fuscum* were identical in both the oxidized and the reduced forms. Therefore, a comparison can be made between the studies here on B. fuscum PCD{} and the crystallographic results for P. putida PCD{}.
(8) Elgren, T. E.; Orville, A. M.; Kelly, K. A.; Lipscomb, J. D.; Ohlendorf, D. H.; Que, L., Jr. *Biochemistry* **1997**, *36*, 11504−11513.
(9) Frazee, R. W.; Orville, A. M.; Dolbeare, K. B.; Yu, H.; Ohlendorf, D. H.; Lipscomb, J. D. *Biochemistry* **1998**, *37*, 2131−2144.
(10) Orville, A. M.; Lipscomb, J. D.; Ohlendorf, D. H. *Biochemistry* **1997**, *36*, 10052−10066.
(11) Orville, A. M.; Elango, N.; Lipscomb, J. D.; Ohlendorf, D. H. *Biochemistry* **1997**, *36*, 10039−10051.
(12) Ohlendorf, D. H.; Orville, A. M.; Lipscomb, J. D. *J. Mol. Biol.* **1994**, *244*, 586−608.
(13) Vetting, M. W.; D'Argenio, D. A.; Ornston, L. N.; Ohlendorf, D. H. *Biochemistry* **2000**, *39*, 7943−7955.
(14) True, A. E.; Orville, A. M.; Pearce, L. L.; Lipscomb, J. D.; Que, L., Jr. *Biochemistry* **1990**, *29*, 10847−10854.
(15) Davis, M. I.; Wasinger, E. C.; Westre, T. E.; Zaleski, J. M.; Orville, A. M.; Lipscomb, J. D.; Hedman, B.; Hodgson, K. O.; Solomon, E. I. *Inorg. Chem.* **1999**, *38*, 3676−3683.
(16) Davis, M. I.; Orville, A. M.; Neese, F.; Zaleski, J. M.; Lipscomb, J. D.; Solomon, E. I. *J. Am. Chem. Soc.* **2002**, *124*, 602−614.
(17) Bull, C.; Ballou, D. P.; Otsuka, S. *J. Biol. Chem.* **1981**, *256*, 12681−12686.
(18) Arciero, D. M.; Orville, A. M.; Lipscomb, J. D. *J. Biol. Chem.* **1983**, *258*, 14981−14991.
(19) Westcott, B. L.; Enemark, J. H. Transition Metal Nitrosyls. In *Inorganic Electronic Structure and Spectroscopy*, Volume II: Applications and Case Studies; Solomon, E. I., Lever, A. B. P., Eds.; John Wiley and Sons: New York, 1999; pp 403−450.
(20) Brown, C. A.; Pavlosky, M. A.; Westre, T. E.; Zhang, Y.; Hedman, B.; Hodgson, K. O.; Solomon, E. I. *J. Am. Chem. Soc.* **1995**, *117*, 715−732.
(21) Orville, A. M.; Lipscomb, J. D. *J. Biol. Chem.* **1993**, *268*, 8596−8607.
(22) Orville, A. M.; Lipscomb, J. D. *Biochemistry* **1997**, *36*, 14044−14055.
(23) Zhang, Y.; Pavlosky, M. A.; Brown, C. A.; Westre, T. E.; Hedman, B.; Hodgson, K. O.; Solomon, E. I. *J. Am. Chem. Soc.* **1992**, *114*, 9189−9191.
(24) Westre, T. E.; Di Cicco, A.; Filipponi, A.; Natoli, C. R.; Hedman, B.; Solomon, E. I.; Hodgson, K. O. *J. Am. Chem. Soc.* **1994**, *116*, 6757−6768.
(25) Rich, P. R.; Salerno, J. C.; Leigh, J. S.; Bonner, W. D. *FEBS Lett.* **1978**, *93*, 323−326.
(26) Shepherd, R. E.; Sweetland, M. A.; Junker, D. E. *J. Inorg. Biochem.* **1997**, *65*, 1−14.

performed a detailed geometric and electronic structure analysis of $[Fe(EDTA)NO]^{2-}$, which can be used to develop an understanding of the {FeNO}^{7} systems studied here.[20] The EPR spectrum of $[Fe(EDTA)NO]^{2-}$ ($g_\perp$ splits into 4.1 and 3.9, giving an *E/D* of 0.016) indicates that the site is more axial than either Fe^{III}PCD{NO^-} or Fe^{III}PCD{PCA,NO^-}. The lowest energy magnetic circular dichroism (MCD) and UV−vis absorption (Abs) transitions are at 12 900, 15 120, 17 400, 19 650, and 22 580 cm^{-1}. The variable-temperature variable-field (VTVH) MCD saturation data for the 22 580- and 15 120-cm^{-1} transitions of $[Fe(EDTA)NO]^{2-}$ are equivalent and the data taken at different temperatures nearly superimpose. The 12 900- and 15 120-cm^{-1} transitions are assigned to $^6A_1$ to $^4T_1$ and $^6A_1$ to $^4T_2$ spin forbidden d → d transitions, respectively. The next three transitions are from the NO^- in-plane (ip) π^* to Fe(III) $d_{x^2-y^2}$, NO^- in-plane $2\pi^*$ to Fe(III) d_{xz}, and NO^- out-of-plane (op) $2\pi^*$ to Fe(III) d_{yz} charge transfer (CT) transitions, where the bent Fe−NO unit (156° angle) is in the *xz* plane. The peak at 22 580 cm^{-1} is the most intense since the transition involves a ligand out-of-plane π to metal d_π CT and orbital overlap is the highest.[20]

In this study, XAS, MCD, VTVH MCD, and Abs spectroscopies have been used to study the geometric and electronic structure of the Fe^{III}PCD{NO^-} and Fe^{III}PCD{PCA,NO^-} complexes. Using the recently developed methodology,[28−31] VTVH MCD data can be used to obtain the polarization of the associated electronic transitions relative to the principal axes of the zero-field tensor, providing polarization information on a randomly oriented sample where previously such data were possible only with single-crystal absorption spectroscopy. The nature of the two NO complexes and their spectroscopic features were examined to gain insight into the effect of other ligands on the Fe−NO bond. A comparison is made among $[Fe(EDTA)NO]^{2-}$, Fe^{III}PCD{NO^-}, and Fe^{III}PCD{PCA,NO^-}, which shows that the Fe−NO bond in both protein complexes is unusually long and weak. The only other protein or model system where such a long, weak Fe−NO bond has been observed is in isopenicillin *N*-synthase (IPNS) when substrate (δ-(L-α-aminoadipoyl)-L-cysteinyl-D-valine or ACV) is bound.[32] The catalytic relevance of strong endogenous ligand donor binding on O_2 activation as revealed by the {FeNO}^{7} active site complexes is considered.

Experimental Section

Sample Preparation. All commercial reagents were of the highest grade available and were used without further purification unless noted. Protocatechuate 3,4-dioxygenase from *Brevibacterium fuscum* was purified as previously reported,[33,34] stored at −80 °C, and thawed immediately prior to use. The EPR spectra of the nitrosyl complexes were identical to those previously reported with the exception of not having the small $g = 4.3$ contaminant.[21] The 100 mM MOPS buffer (3-[*N*-morpholino]propane-sulfonic acid; Sigma) was adjusted to pH 7.0 with NaOH (Sigma). Protocatechuate (3,4-dihydroxybenzoic acid, Aldrich, PCA) was purified by sublimation by heating the sample under vacuum in a flask equipped with a coldfinger-cooled by dry ice. Once purified, it was stored under N_2 in the dark. The NO gas (Matheson) was scrubbed by passing it through a NaOH drying tube to remove other NO_x species.

All samples were prepared under strict anaerobic conditions. Fe^{III}PCD{} was rigorously degassed at 4 °C in a Teflon-stoppered flask by evacuating and filling 20 times with Ar that had been passed over copper catalyst (BASF Inc.) to remove residual O_2. Sodium dithionite (Sigma) was prepared just prior to use with degassed (Ar purge) deionized H_2O. In a nitrogen glovebox, a small aliquot of sodium dithionite (≈7-fold excess equiv) was added to PCD (maintained at 4 °C) and allowed to react until the color of the enzyme bleached from the characteristic red color ($\lambda_{max} = 460$ nm, <30 min); this reduction is reversible.[35] For substrate-containing samples, a small aliquot of a substrate solution (pH adjusted anaerobically to avoid air oxidation) was added anaerobically to Fe^{II}PCD{} to give 25-fold excess substrate and incubated for 15 min. Then the sample was transferred into an N_2-filled glovebag. NO gas was blown in the headspace of the septum-sealed flask maintained at 4 °C and the sample was stirred periodically to ensure proper mixing. The reaction was continued until there was no additional development of yellow color characteristic of the nitrosyl complex, usually within 15 min. For many of the experiments, one large batch was made and then EPR, MCD, and XAS sample cells were loaded simultaneously and frozen quickly in liquid N_2. The XAS samples were 2−3 mM in iron and the MCD samples ranged from 0.33 to 2.0 mM in iron. Upon exposure to air, Fe^{III}PCD{NO^-} regains full activity, indicating that the NO does not degrade the enzyme.[18] $[Fe(EDTA)NO]^{2-}$ was prepared as described in ref 17.

For the MCD experiments, 50% (v/v) glycerol, degassed under vacuum by freeze/pump/thaw/heat procedures, was added as a glassing agent. CD and Abs spectra were taken with and without glycerol present to ensure that the protein was unaffected by the glassing agent. The iron concentrations of the samples were 0.33 mM for the UV−visible CD/Abs/MCD and 2.0 mM for the near-IR CD/MCD. MOPS buffer prepared in D_2O (99.9 atom % D; Aldrich) and adjusted to a pD of 6.6 with NaOD (Sigma) and glycerol-d_3 (98 atom % D; Cambridge Isotopes Laboratories) were used to eliminate the hydroxide stretches that dominate the IR absorption spectrum above 1600 nm.

X-ray Absorption Spectroscopy Measurements. XAS samples (2−3 mM in iron) were transferred into Lucite XAS cells with 37-μm Kapton windows and frozen in liquid nitrogen. Data were recorded at the Stanford Synchrotron Radiation Laboratory (SSRL) on unfocused beam line 7-3 during ring conditions of 3 GeV and 50−100 mA. Monochromatism of the radiation was achieved using a Si(220) double-crystal monochromator. Data were measured to $k = 15$ $Å^{-1}$ with 1-mm-high pre-monochromator beam-defining slits, and the monochromator was detuned to 50% at 7987 eV to minimize harmonic contamination. An Oxford Instruments continuous-flow liquid-helium CF1208 cryostat was used to maintain a

(27) Ray, M.; Golombeck, A. P.; Hendrich, M. P.; Yap, G. P. A.; Liable-Sands, L. M.; Rheingold, A. L.; Borovik, A. S. *Inorg. Chem.* **1999**, *38*, 3110−3115.
(28) Neese, F.; Solomon, E. I. *J. Am. Chem. Soc.* **1998**, *120*, 12829−12848.
(29) Neese, F.; Solomon, E. I. *Inorg. Chem.* **1999**, *38*, 1847−1865.
(30) Oganesyan, V. S.; George, S. J.; Cheesman, M. R.; Thomson, A. J. *J. Chem. Phys.* **1999**, *110*, 762−777.
(31) Oganesyan, V. S.; Thomson, A. J. *J. Chem. Phys.* **2000**, *113*, 5003−5017.
(32) Roach, P. L.; Clifton, I. J.; Hensgens, C. M. H.; Shibata, N.; Schofield, C. J.; Hajdu, J.; Baldwin, J. E. *Nature* **1997**, *387*, 827−830.
(33) Whittaker, J. W.; Orville, A. M.; Lipscomb, J. D. *Methods Enzymol.* **1990**, *188*, 82−88.
(34) Whittaker, J. W.; Lipscomb, J. D.; Kent, T. A.; Münck, E. *J. Biol. Chem.* **1984**, *259*, 4466−4475.
(35) Fujisawa, H.; Uyeda, M.; Kojima, Y.; Nozaki, M.; Hayaishi, O. *J. Biol. Chem.* **1972**, *247*, 4414−4421.

constant sample temperature of 10 K. Energies were calibrated using an internal Fe foil standard, assigning the first inflection point to 7111.2 eV.[36] The spectrometer energy resolution was ≈1.4 eV with reproducibility in the edge position of <0.2 eV. The fluorescence signal was monitored using a 13-element Ge solid-state array detector electronically windowed on the Fe Kα signal.[37]

Extended X-ray absorption fine structure (EXAFS) data reduction was performed on the averaged protein spectra according to established methods.[38−41] A smooth pre-edge background was removed from the averaged spectra by fitting a Gaussian polynomial to the pre-edge region and subtracting this polynomial from the entire spectrum. A three-region spline through the EXAFS region was fit and the data normalized. The spline was established to minimize residual low-frequency background but not reduce the EXAFS amplitude as checked by monitoring the Fourier transform of the EXAFS during the fitting and subtraction process. The normalized data were converted to *k*-space, where the photoelectron wave vector, *k*, is defined by $[2m_e(E - E_0)h^2]^{1/2}$, where m_e is the electron mass, *E* is the photon energy, *h* is Planck's constant divided by 2π, and E_0 is the threshold energy of the absorption edge, which was defined to be 7130 eV for the Fe K absorption edge.

Theoretical EXAFS signals $\chi(k)$ were calculated using *FEFF* (version 6) and fit to the data using EXAFSPAK.[42] The structural parameters varied were *R*, the bond distance, σ^2, the bond variance, and E_0, the threshold ($k = 0$ point) shift in eV. The bond variance is related to the Debye−Waller factor, which is a measure of the thermal vibration and static disorder of the absorber−scatterer pair. Data were fit over the range $k = 2-13$ Å^{-1}. Although the threshold energy E_0 was allowed to vary in each fit, it was restricted to a common value for every component in that fit. Coordination numbers were systematically varied in integer steps in the course of the analysis, but were not allowed to vary within a fit. On the basis of studies of complexes of known structures, the uncertainties in final distances are within 0.02 Å. Fits were evaluated by comparing the normalized error for the fits, calculated as the sum of the squares of the differences between experimental and calculated curves divided by the number of points.

The intensities and energies of the 1s → 3d pre-edge features of the protein data were quantified with the fitting program EDG_FIT,[43] which utilizes the double-precision version of the public domain MINPAK fitting library. All spectra were fit over the range 7108−7118 eV. Pseudo-Voigt line shapes of a fixed 50:50 ratio of Lorentzian to Gaussian contribution were used to model pre-edge features and successfully reproduced the spectra. Functions modeling the background contributions to the pre-edge features were chosen empirically to give the best fit and included pseudo-Voigt functions that mimicked shoulders on the rising edge. For all complexes, 8−10 fits were obtained, which equally well reproduced the data and the second derivative with variation in the background function used. A fit was considered acceptable only if it successfully reproduced the data *and* the second derivative of the data. The values reported for the areas of the pre-edge features, where peak area is approximated by the height multiplied by the full-width at half-maximum, are the average of all the pseudo-Voigt functions that successfully fit the feature and its second derivative. To quantify the error, the standard deviations for the peak energies and intensities were calculated from all the pseudo-Voigt functions that fit the pre-edge features from all the successful fits for each sample. To calculate the energy of the edge jump, a straight line was fit through the data of each sample between 7120 and 7125 eV. The reported edge energy for each sample is the energy of that line at a chosen value of 0.6 normalized units.

Electronic Absorption Spectroscopy. UV−visible Abs spectra (200−820 nm) were recorded at room temperature on a HP8452A diode array spectrometer in a 0.5-cm path length quartz anaerobic cuvette. Low-temperature absorption spectra (5 K) were obtained on a Cary 17 spectrometer equipped with a Janis Research Super Vari-temp helium cryogenic dewar mounted in the light path.

Electron Paramagnetic Resonance Spectroscopy. EPR spectra were recorded at 5 K on a Bruker 220-D SRC spectrometer equipped with an Air Products model LTR Helitran liquid-helium cryostat. The microwave frequencies (9.55 GHz) were measured with a Hewlett-Packard x532B frequency meter. EPR simulations were generated using the Bruker programs WINEPR and SimFonia. For the simulations the number of θ segments are 300, the number of φ segments is 200, the line widths are each 10, and the Lorentzian-to-Gaussian ratio is 1. The He-EPR spectra of Fe^{III}PCD{NO^-} and Fe^{III}PCD{PCA,NO^-} indicate that the species formed were the same $S = {}^3/_2$ species previously observed[21] with the refinement that there is no signal at $g = 4.3$ from Fe^{III}PCD{} or Fe^{III}PCD{PCA}.

Circular Dichroism and Magnetic Circular Dichroism Spectroscopy. The near-IR data were collected on a Jasco J-200D (600−2140 nm) spectropolarimeter with a liquid-N_2-cooled InSb detector. The J-200D is equipped with an Oxford Instruments SM4000-7 Tesla (T) superconducting magnet/cryostat capable of fields up to 7 T and temperatures down to 1.5 K. The UV/visible data were collected on a Jasco J-500C (200−1060 nm) with an extended S-20 and S-1 Photomultiplier tube (Hammamatsu) or on a Jasco J-810 (180−1060 nm). The J-500C and Jasco J-810 are equipped with an Oxford Instruments SM4-7 T superconducting magnet/cryostat capable of fields up to 7 T and temperatures down to 1.5 K.

CD samples were prepared in a 0.5-cm path length cuvette and were kept at 4 °C at all times with a circulating cooling bath attached to the sample holder. Buffer and cell baselines were subtracted from the raw protein CD spectra. Low-temperature (1.6−50.2 K) MCD spectra were obtained in a copper MCD sample cell with two Infrasil quartz disks sandwiching a 3-mm-thick neoprene O-ring spacer into which the sample was injected. MCD samples were quickly frozen in liquid N_2 immediately after preparation. The depolarization of the frozen MCD sample, checked by measuring the CD spectrum of a nickel (+)-tartarate solution placed before and after the sample, was <5%.[44]

The MCD spectra were corrected for the natural CD and zero-field baseline effects caused by strain in the glasses by subtracting

(36) Scott, R. A.; Hahn, J. E.; Doniach, S.; Freeman, H. C.; Hodgson, K. O. *J. Am. Chem. Soc.* **1982**, *104*, 5364−5369.
(37) Cramer, S. P.; Tench, O.; Yochum, M.; George, G. N. *Nucl. Instrum. Methods Phys. Rev.* **1988**, *A266*, 586−591.
(38) Cramer, S. P.; Hodgson, K. O.; Stiefel, E. I.; Newton, W. E. *J. Am. Chem. Soc.* **1978**, *100*, 2748−2761.
(39) Cramer, S. P.; Hodgson, K. O. *Prog. Inorg. Chem.* **1979**, *25*, 1−39.
(40) Scott, R. A. *Methods Enzymol.* **1985**, *117*, 414−459.
(41) Zhang, H. H.; Hedman, B.; Hodgson, K. O. X-ray Absorption Spectroscopy and EXAFS Analysis: The Multiple-Scattering Method and Applications in Inorganic and Bioinorganic Chemistry. In *Inorganic Electronic Structure and Spectroscopy*; Solomon, E. I., Lever, A. B. P., Eds.; John Wiley & Sons: New York, 1999; pp 513−554.
(42) George, G. N. *EXAFSPAK*; Stanford Synchrotron Radiation Laboratory, Stanford Linear Accelerator Center, Stanford University: Stanford, CA.
(43) George, G. N. *EDG_FIT*; Stanford Synchrotron Radiation Laboratory, Stanford Linear Accelerator Center, Stanford University: Stanford, CA.
(44) Browett, W. R.; Fucaloro, A. F.; Morgan, T. V.; Stephens, P. J. *J. Am. Chem. Soc.* **1983**, *105*, 1868−1872.

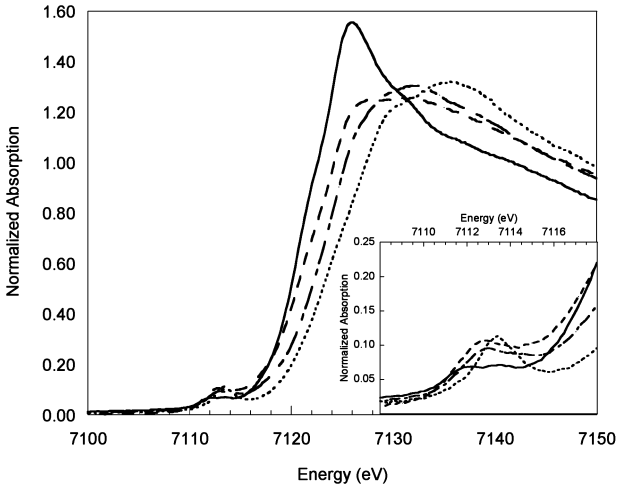

Figure 1. Edge energies of intradiol dioxygenase sites: $Fe^{II}PCD\{\}$ (—); $Fe^{III}PCD\{PCA,NO^-\}$ (- - -); $Fe^{III}PCD\{NO^-\}$ (- − -); $Fe^{III}PCD\{\}$ (···). Inset: pre-edge region of $Fe^{II}PCD\{\}$ (—); $Fe^{III}PCD\{PCA,NO^-\}$ (- - -); $Fe^{III}PCD\{NO^-\}$ (- − -); $Fe^{III}PCD\{\}$ (···).

the 0-T scans from each of the field scans at a given temperature. The Abs, CD, and MCD spectra were iteratively fit to Gaussian band shapes by using a modified Levenberg−Marquardt constrained least-squares fitting routine. For VTVH MCD spectroscopy, a calibrated carbon-glass or Cernox resistor (Lakeshore Cryotronics, calibrated 1.5−300 K) inserted in the sample cell was used to accurately measure the temperature of the sample. VTVH MCD data were analyzed using the theory and associated fitting program developed in ref 27.

Results and Analysis

A. XAS Edge. XAS 1s → continuum edge energies are indicative of the effective charge of the photoabsorbing atom and have been extensively used to determine oxidation states in model complexes and protein sites.[45−49] In the case of iron complexes, ferric sites are found to have edges at higher energy than their ferrous counterparts with similar ligation because of their increased effective nuclear charge. The edge energy can consequently be used as a diagnostic tool for the degree of charge donation in a series of metal complexes with closely related ligands.

The iron K-edges of the intradiol dioxygenase samples are shown in Figure 1. $Fe^{III}PCD\{\}$ with an active site consisting of two tyrosinate ligands, one hydroxide ligand, and two histidine ligands is found to have an edge energy of 7124.0 eV (0.6 normalized intensity units), 2.6 eV lower than that of a hexaquo iron(III) model complex (not shown).[50] As rising edge inflection points are often not possible to determine due to the presence of varying transition superimposed on the edge, an energy above where such effects dominate was chosen. While the choice of 0.6 normalized units at which to assign the edge energy is arbitrary, it allows relative edge energy comparisons, as the ordering of edge positions remains constant over the range 0.3−1.2 normalized units. Thus, the endogenous ligands of $Fe^{III}PCD\{\}$ clearly transfer a significant amount of charge to the iron, lowering the effective nuclear charge of the metal. Binding of NO to the enzyme without substrate shifts the edge to 7122.7 eV relative to $Fe^{III}PCD\{\}$, indicating an additional decrease in effective charge on the iron atom. Binding of both substrate and nitrosyl to the active site in the $Fe^{III}PCD\{PCA,NO^-\}$ complex shifts the edge to 7121.2 eV, almost 3 eV lower in energy relative to $Fe^{III}PCD\{\}$. For comparison, the edge energy of $Fe^{II}PCD\{\}$ is 7120.5 eV.[15]

Table 1. Pre-edge Energies and Intensities (with Standard Deviations) of $Fe^{III}PCD\{\}$, $Fe^{III}PCD\{NO^-\}$, and $Fe^{III}PCD\{PCA,NO^-\}$

	edge energy (eV)	pre-edge energy (eV)	intensity	total area
$Fe^{III}PCD\{\}$	7124.0	7113.4	16.4 (1.7)	16.4 (1.7)
$Fe^{III}PCD\{NO^-\}$	7122.7	7112.7	14.4 (0.3)	
		7114.5	2.9 (0.5)	17.3 (0.8)
$Fe^{III}PCD\{PCA,NO^-\}$	7121.2	7112.5	18.7 (1.3)	
		7113.9	1.7 (0.4)	
		7114.9	1.6 (0.4)	22.0 (1.3)

B. XAS Pre-edge. Model studies have shown that pre-edge shape and intensity patterns can be correlated to coordination number and geometry.[45,47,50] The 1s → 3d pre-edge features are formally electric dipole forbidden, but gain intensity through an electric quadrupole transition, and are therefore observed to be weak in centrosymmetric complexes. Typical six-coordinate ferric complexes have a pre-edge intensity of ≈4.9 units distributed over two features split by approximately 1.4 eV. It has been shown, however, that loss of centrosymmetry results in additional pre-edge intensity due to 4p orbital mixing into the unoccupied and half-occupied 3d orbitals.[47,50,51] Since the 1s → 4p electric dipole transition is ≈100-fold more efficient than the quadrupole transition,[52,53] only a few percent 4p mixing is necessary to greatly enhance the intensity of the pre-edge feature.[50] Non-centrosymmetric complexes are therefore observed to have a higher pre-edge intensity: five-coordinate ferric models typically display two features with a total pre-edge intensity of ≈14 units, and tetrahedral ferric model data are well fit by a single feature (due to the reduced ligand field strength) having ≈20 units of intensity. Protein active sites with dissimilar ligation, variations in bond distances, and noncoincidence of the molecular axes with any of the ligands' bonding orbitals will therefore have an increased pre-edge intensity relative to models with similar oxidation state and geometry due to the additional 1s → 4p dipole contribution to the pre-edge.

The pre-edge energies and intensities for the individual features of the $Fe^{III}PCD\{\}$, $Fe^{III}PCD\{NO^-\}$, and $Fe^{III}PCD\{PCA,NO^-\}$ complexes are listed in Table 1 (see inset,

(45) Shulman, R. G.; Yafet, Y.; Eisenberger, P.; Blumberg, W. E. *Proc. Natl. Acad. Sci. U.S.A.* **1976**, *73*, 1384−1388.
(46) Cramer, S. P.; Eccles, T. K.; Kutzler, F. W.; Hodgson, K. O. *J. Am. Chem. Soc.* **1976**, *98*, 1287−1288.
(47) Roe, A. L.; Schneider, D. J.; Mayer, R. J.; Pyrz, J. W.; Widom, J.; Que, L., Jr. *J. Am. Chem. Soc.* **1984**, *106*, 1676−1681.
(48) Wong, J.; Lytle, F. W.; Messmer, R. P.; Maylotte, D. H. *Phys. Rev. B* **1984**, *30*, 5596−5610.
(49) Kau, L.-S.; Spira-Solomon, D. J.; Penner-Hahn, J. E.; Hodgson, K. O.; Solomon, E. I. *J. Am. Chem. Soc.* **1987**, *109*, 6433−6442.
(50) Westre, T. E.; Kennepohl, P.; DeWitt, J. G.; Hedman, B.; Hodgson, K. O.; Solomon, E. I. *J. Am. Chem. Soc.* **1997**, *119*, 6297−6314.
(51) Randall, C. R.; Shu, L.; Chiou, Y.-M.; Hagen, K. S.; Ito, M.; Kitajima, N.; Lachicotte, R. J.; Zang, Y.; Que, L., Jr. *Inorg. Chem.* **1995**, *34*, 1036−1039.
(52) Bair, R. A.; Goddard, W. A. *Phys. Rev.* **1980**, *B22*, 2767−2776.
(53) Brouder, C. J. *J. Phys.: Condens. Matter* **1990**, *2*, 701−738.

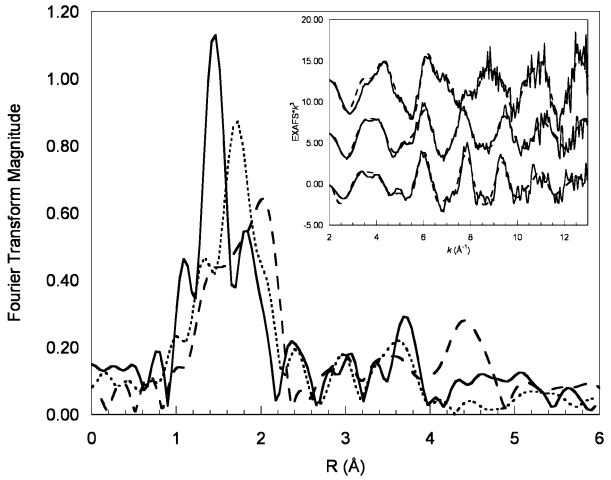

Figure 2. (a) Fourier transform of data for $Fe^{III}PCD\{\}$ (—), $Fe^{III}PCD\{NO^-\}$ (···), and $Fe^{III}PCD\{PCA,NO^-\}$ (- - -). Inset: EXAFS data (—) and fits to the data (- - -) of $Fe^{III}PCD\{\}$ (top), $Fe^{III}PCD\{NO^-\}$ (middle), and $Fe^{III}PCD\{PCA,NO^-\}$ (bottom). Data for $Fe^{III}PCD\{\}$ and $Fe^{III}PCD\{NO^-\}$ have been offset by 12 and 6 units, respectively.

Figure 1). A single feature at 7113.4 eV with an intensity of 16.4 units adequately reproduced the pre-edge data and the second derivative of the ferric enzyme. $Fe^{III}PCD\{\}$ is known to be five-coordinate from the available crystal structure.[12,54] Thus, the intensity of $Fe^{III}PCD\{\}$ can be used as a standard for five-coordinate systems with similar ligation. Binding of NO to $Fe^{II}PCD\{\}$ results in a redistribution of pre-edge intensity in which two features are required at 7112.7 and 7114.5 eV to fit the data of the $Fe^{III}PCD\{NO^-\}$ complex. The lower energy feature comprises the majority of the intensity with 14.4 units; the higher energy feature is much weaker with 2.9 units of intensity. Finally, three features are required to fit the data and second derivative of the $Fe^{III}PCD\{PCA,NO^-\}$ complex at 7112.5, 7113.9, and 7114.9 eV with 18.7, 1.7, and 1.6 units of intensity, respectively.

Typically, $\{FeNO\}^7$ complexes are characterized by short iron−nitrosyl bonds. The short iron−nitrosyl interaction induces 4p mixing into the d_{z^2} orbital and dramatically increases the pre-edge intensity relative to complexes of similar coordination number.[20,50] For the [Fe(salen)(NO)] and $[Fe(Me_3tacn)(NO)(N_3)_2]$ complexes, the pre-edge intensity increased by ≈10 units relative to their Fe^{III} analogues. In both the $Fe^{III}PCD\{NO^-\}$ and $Fe^{III}PCD\{PCA,NO^-\}$ complexes the total pre-edge intensity is similar to that of $Fe^{III}PCD\{\}$ (17.3 and 22.0 versus 16.4 units of intensity, respectively). While small increases in pre-edge intensity are observed, the dramatic increase typical of strong iron−nitrosyl bonding is not present. This indicates a weaker Fe−NO bond in this system relative to the $\{FeNO\}^7$ model sites with innocent (i.e., less covalent) ligands.

C. EXAFS. The EXAFS and respective Fourier-transformed data of the $Fe^{III}PCD\{\}$, $Fe^{III}PCD\{NO^-\}$, and $Fe^{III}PCD\{PCA,NO^-\}$ complexes are given in Figure 2. Previously published XAS data of $Fe^{III}PCD\{\}$ suggested a split first-coordination sphere likely consisting of three ligands at 1.90 Å and two ligands at 2.08 Å, and a coordination-weighted averaged distance of 1.97 Å.[14] For direct comparison with the $Fe^{III}PCD\{NO^-\}$ complex, XAS data (Figure 2) of $Fe^{III}PCD\{\}$ have been remeasured under identical conditions[15] and are reproduced in Table 2. Similar to the earlier study,[14] two first-shell components are required to fit the data at 1.88 and 2.10 Å, with an average distance of 1.97 Å. It is clear from the EXAFS data of $Fe^{III}PCD\{\}$ and $Fe^{III}PCD\{NO^-\}$ (Figure 2, inset) that the data for $Fe^{III}PCD\{NO^-\}$ is of higher frequency than that of the ferric enzyme, implying a longer average distance in the $Fe^{III}PCD\{NO^-\}$ complex. This is further supported by visual inspection of the Fourier transforms of the data (Figure 2) wherein the main first-coordination sphere features have moved to longer distances for $Fe^{III}PCD\{NO^-\}$ relative to $Fe^{III}PCD\{\}$ coincident with a redistribution of intensity in the first two peaks. Two components are required to fit the first-coordination sphere of $Fe^{III}PCD\{NO^-\}$, one ligand at 1.91 Å and four ligands at 2.11 Å, with the average distance being 2.07 Å (Table 2). Removal of either component results in a lower quality fit to the EXAFS and Fourier transform of the data. Selected carbon single- and multiple-scattering components representing prominent averages of contributions from the histidine and tyrosinate rings complete the EXAFS fit, where the differences in single-scattering and multiple-scattering distances reflect the two different types of paths.

Fits to the $Fe^{III}PCD\{NO^-\}$ EXAFS data including an NO multiple-scattering component were unsuccessful. The Fe−NO distance and the Fe−N−O bond angle were systematically varied by 0.1 Å and 10°, respectively, and the resulting starting models used to recalculate EXAFS phase and amplitude components in *FEFF*. In the few cases where the addition of the multiple-scattering wave did not degrade the fit quality, the Fe−N−O angle was calculated to be ≤150°. In all cases, including the multiple scattering components did not improve the fit and therefore cannot be justified in the fits.

The EXAFS data of the $Fe^{III}PCD\{PCA,NO^-\}$ complex is shifted to slightly higher frequency than the data of $Fe^{III}PCD\{NO^-\}$ (Figure 2, inset), especially at higher k values. This is also observed in the Fourier transform of the data (Figure 2) with greater intensity at ≈2 Å. This again indicates a longer average first-shell distance (2.19 Å), which is illustrated by the best fit to the EXAFS data. Three components are required to fit the first-coordination sphere of the $Fe^{III}PCD\{PCA,NO^-\}$ complex, presented in Table 2. The best fit to the data is found with one ligand at 1.93 Å, three ligands at 2.10 Å, and finally two additional ligands at 2.44 Å. Reducing the coordination number in any of the three component shells results in a worse fit both visually and statistically (i.e., higher error value) or reduces the Debye−Waller factor of that shell to an unreasonably small or negative number. Thus, EXAFS analysis indicates that the best fit to the data is a six-coordinate active site for $Fe^{III}PCD\{PCA,NO^-\}$. As with the $Fe^{III}PCD\{NO^-\}$ complex above, additional components are required to fit the carbon single scattering and multiple scattering from the histidine, tyrosinate, and catecholate ligands as listed in Table 2. As

(54) Ohlendorf, D. H.; Lipscomb, J. D.; Weber, P. C. *Nature* **1988**, *336*, 403−405.

Table 2. EXAFS Fit Results for $Fe^{III}PCD\{\}$, $Fe^{III}PCD\{NO^-\}$, and $Fe^{III}PCD\{PCA,NO^-\}$

	$Fe^{III}PCD\{\}$			$Fe^{III}PCD\{NO^-\}$			$Fe^{III}PCD\{PCA,NO^-\}$		
	CN	R (Å)	σ^2 (Å^2)	CN	R (Å)	σ^2 (Å^2)	CN	R (Å)	σ^2 (Å^2)
Fe−N/O	3	1.88	0.00220	1	1.91	0.00323	1	1.93	.00288
Fe−N/O	2	2.10	0.00114	4	2.11	0.00276	3	2.10	0.00328
Fe−N/O							2	2.44	0.00173
Fe−C/N SS[a]	4	3.01	0.00702	4	3.00	0.01008	4	2.82	0.00989
Fe−C MS[a]	6	3.33	0.00104	6	3.24	0.00705	7	3.39	0.00317
Fe−C MS	6	4.30	0.00737	6	4.33	0.00655	8	4.31	0.00800
avg. Fe−N/O R (Å)		1.97			2.07			2.19	
error[b]		0.91			0.40			0.50	

[a] SS: single scattering. MS: multiple scattering. [b] Error is defined as $F = \sum[(\chi_{exp} - \chi_{obsd})^2 k^6]/\sum[\chi^2_{exp} k^6]$.

with the $Fe^{III}PCD\{NO^-\}$ complex, a multiple-scattering wave resulting from the NO ligand could not be included in the fit to the data (not shown). It should be noted that a new feature has appeared in the non-phase-shift-corrected Fourier transform of the $Fe^{III}PCD\{PCA,NO^-\}$ complex at ≈4.5 Å, presumably due to the presence of substrate, although a detailed analysis of this feature is precluded by the high noise level of the data.

The average bond lengths of $Fe^{III}PCD\{NO^-\}$ and $Fe^{III}PCD\{PCA,NO^-\}$ (2.07 and 2.19 Å, respectively) are significantly longer than that of $Fe^{III}PCD\{\}$ (1.97 Å). This is consistent with the shift in edge energies of these complexes (vide supra) and is further indication of charge donation to iron in the NO complexes. Furthermore, most $\{FeNO\}^7$ model complexes are found to have a short, strong Fe−NO bond of ≈1.75 Å.[20,24,27,55,56] In $Fe^{III}PCD\{NO^-\}$ the Fe−NO bond must be at least ≈1.91 Å, almost 0.2 Å longer than standard Fe−NO model complexes. In the $Fe^{III}PCD\{PCA,NO^-\}$ complex, the minimum bond length is slightly longer at ≈1.93 Å. The lack of a short bond in the $Fe^{III}PCD\{NO^-\}$ and $Fe^{III}PCD\{PCA,NO^-\}$ EXAFS fits and the lack of an identifiable FeNO multiple-scattering component implies a divergent $\{FeNO\}^7$ structural unit in the protein $\{FeNO\}^7$ sites relative to model complexes, which derives from the strong CT from the endogenous protein ligands observable in the XAS edges.

D. Magnetic Circular Dichroism Spectroscopy. 1. $[Fe(EDTA)NO]^{2-}$. VTVH MCD data were collected previously for $[Fe(EDTA)NO]^{2-}$.[20] Current methodology now allows these data to be analyzed to obtain the transition polarizations for randomly oriented molecules in frozen solution. This information is important in assigning the transitions and in elucidating electronic structure. VTVH MCD data (Figure 3, inset) were collected at a variety of temperatures and fields for the two main bands in $[Fe(EDTA)NO]^{2-}$, as indicated by arrows in Figure 3. The nesting observed for the different isotherms is expected for an $S = {}^3/_2$ system and the transitions are identified as MCD C-terms.

The VTVH MCD data were fit using an approach based on the spin-Hamiltonian that relates the nonlinear MCD behavior to both transition polarization and spin−orbit coupling for systems with $S \geq {}^1/_2$ in low-symmetry molecular

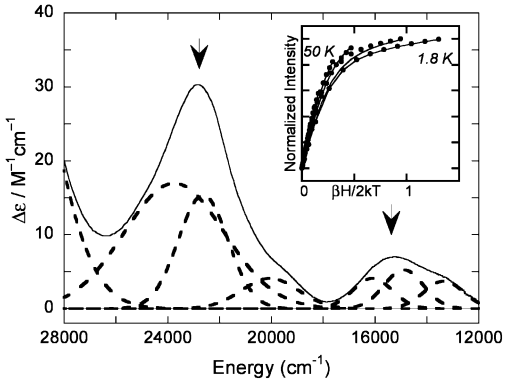

Figure 3. Gaussian resolution (- - -) of $[Fe(EDTA)NO]^{2-}$ MCD spectra at 5 K and 7 T (—). There are no MCD transitions between 5000 and 12 000 cm^{-1} and this region was omitted for clarity. The inset shows the VTVH MCD data and fit for the transition at 22 580 cm^{-1} that is identical to that at 15 120 cm^{-1} (not shown).

environments.[29] If the spin-Hamiltonian parameters D, E/D, g_x, g_y, and g_z are fixed from EPR, then the effective transition moment products M^{eff}_{xy}, M^{eff}_{xz}, and M^{eff}_{yz} can be determined from eq 1.[29,57] From the effective transition dipole products,

$$\frac{\Delta\epsilon}{E} = \frac{\gamma}{4\pi S}\int_0^{\pi}\int_0^{2\pi}\sum_i N_i(l_x\langle S_x\rangle_i M^{eff}_{yz} + l_y\langle S_y\rangle_i M^{eff}_{xz} + l_z\langle S_z\rangle_i M^{eff}_{xy})\sin\theta\,d\theta\,d\phi r \quad (1)$$

the percent polarization along the zero-field splitting (ZFS) tensor axes can be approximated for each transition (eq 2; with cyclic permutations of the indices for the remaining two directions).[29]

$$\%x = 100 \times \left(\frac{(M^{eff}_{xy}M^{eff}_{xz})^2}{(M^{eff}_{xy}M^{eff}_{xz})^2 + (M^{eff}_{xy}M^{eff}_{yz})^2 + (M^{eff}_{yz}M^{eff}_{xz})^2}\right) \quad (2)$$

The VTVH data for $[Fe(EDTA)NO]^{2-}$ were fit using $D = +12$ cm^{-1} [20] (Figure 3, inset) and the transitions were found to be z-polarized. This was predicted by Brown et al. for this complex since these transitions are assigned as NO^- to Fe(III) CT transitions and should be polarized along this bond, and the Fe−NO direction is the unique strong direction

(55) Chiou, Y.-M.; Que, L., Jr. *Inorg. Chem.* **1995**, *34*, 3270−3278.
(56) Hauser, C.; Glaser, T.; Bill, E.; Weyhermüller, T.; Wieghardt, K. *J. Am. Chem. Soc.* **2000**, *122*, 4352−4365.

(57) Here x, y, and z refer to the principal axes of the D or ZFS tensor; $M^{eff}_{ij} = m_i^{AJ} m_j^{AK} L_z^{KJ} \Delta_{KJ}^{-1}$, the transition from A to J is i-polarized, and the transition from A to K is j-polarized; L represents the spin−orbit coupling component; Δ is the energy separation of the excited state and single intermediate state; g is a collection of constants; N_i is the Boltzmann population of the ith magnetic ground-state sublevel and $\langle S\rangle_i$ is its spin expectation value in the direction indicated; l is a unit vector in the field direction; and θ and ϕ are the standard polar angles.

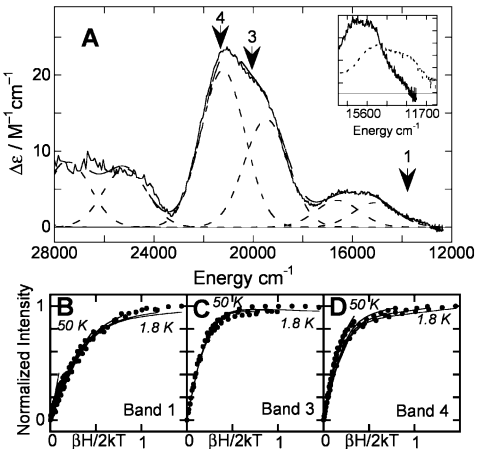

Figure 4. (A) Gaussian resolution (- - -) of the $Fe^{III}PCD\{NO^-\}$ MCD spectra (—) at 5 K and 7 T where the arrows indicate where VTVH MCD data were taken. There are no CD or MCD transitions between 5000 and 12 000 cm^{-1} and this region was omitted for clarity. The inset shows the d → d region for PCD{NO} (—) and $[Fe(EDTA)NO]^{2-}$ (- - -). Bottom: VTVH MCD data for $Fe^{III}PCD\{NO^-\}$ collected between 0 and 7 T and between 1.8 and 50 K at (B) 13 700 cm^{-1} band 1, (C) 20 300 cm^{-1} band 3, and (D) 21 190 cm^{-1} band 4.

Table 3. Gaussian Resolution and Experimental Parameters for the Seven Observed Transitions of $Fe^{III}PCD\{NO^-\}$

band	abs energy (cm^{-1})	ϵ ($mM^{-1}\,cm^{-1}$)	f_{exp}[a]	MCD energy (cm^{-1})	$\Delta\epsilon$ ($M^{-1}\,cm^{-1}$)
1	15 300	0.30	0.0039	15 080	3.2
2	16 590	0.40	0.0052	16 600	3.5
3	18 420	0.40	0.0052	19 470	14.2
4	21 300	1.70	0.022	21 220	20.6
5	25 160	1.72	0.022	25 160	7.7
6	27 480	1.31	0.017	27 440	8.6
7	30 030	2.30	0.030		

[a] The experimental oscillator strengths (f_{exp}) were calculated according to the approximation $f_{exp} = 4.61 \times 10^{-9} * \epsilon_{max}\nu_{1/2}$ (where ϵ_{max} is expressed in $M^{-1}\,cm^{-1}$ and the $\nu_{1/2}$ is expressed in cm^{-1}).

in $[Fe(EDTA)NO]^{2-}$ defining the principal direction of the ZFS tensor.[20,58]

2. 3,4-PCD{NO}. The low-temperature (LT) MCD spectrum for $Fe^{III}PCD\{NO^-\}$ is shown in Figure 4A. The Gaussian fitting of MCD and Abs data indicates that there are seven transitions needed to fit the region from 5000 to 28 000 cm^{-1}. Since no peaks were observed below 11 500 cm^{-1}, there is no unreacted $Fe^{II}PCD\{\}$ present which would have transitions at 8433 and 10 466 cm^{-1}.[15] The energies, full-width at half-maximum ($\nu_{1/2}$), Abs ϵ, MCD $\Delta\epsilon$, and experimental oscillator strengths for $Fe^{III}PCD\{NO^-\}$ are given in Table 3. Bands 1 and 2 have low intensity in Abs (see Supporting Information) relative to MCD, indicating that these are d → d transitions. The other bands are significantly more intense in absorption (smaller *C*/*D*, where *C* quantitates the LT MCD intensity and *D* quantitates the Abs intensity) and hence can be assigned as ligand-to-metal charge-transfer (LMCT) transitions (vide infra).[59]

VTVH data were collected for bands 1, 3, and 4 (Figure 4B,C,D) and fit using the methodology described above. Since an estimate of *D* for $Fe^{III}PCD\{NO^-\}$ was not available

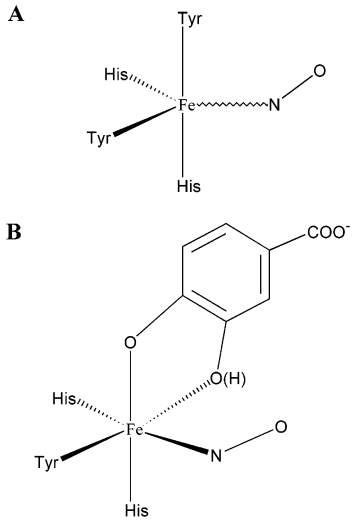

Figure 5. Spectroscopically effective structures for (A) $Fe^{III}PCD\{NO^-\}$ and (B) $Fe^{III}PCD\{PCA,NO^-\}$. The catecholate can either be the monoanion or the dianion depending on the pK_a at the $Fe^{III}-NO^-$ site.

Table 4. Effective Transition Moments from the VTVH MCD Data of $Fe^{III}PCD\{NO^-\}$ and $Fe^{III}PCD\{PCA,NO^-\}$

	M_{xy}	M_{xz}	M_{yz}		M_{xy}	M_{xz}	M_{yz}
$Fe^{III}PCD\{NO^-\}$				$Fe^{III}PCD\{PCA,NO^-\}$			
band 1 + 4	−4.7	2.0	1.3	band 1	0.22	1.1	0.50
band 3	1.5	7.5	−6.9	band 2	−1.0	1.7	0.28
				band 3 + 5	2.1	1.2	−0.50
				band 4	0.11	0.76	1.0

from EPR, a *D*-value was obtained from fitting the VTVH data. The *D*-value was varied from 10 to 25 cm^{-1}, each M_{ij} was varied from +2 to −2 while allowing the other two parameters to float, and the fit values reached a minimum at $D = +22 \pm 3$ cm^{-1}. The effective transition moments, M_{xy}^{eff}, M_{yz}^{eff}, and M_{xz}^{eff}, observed are given in Table 4 and show that bands 1 and 4 are *xy*-polarized, whereas band 3 is *z*-polarized.

With correlation of the MCD data with quantum calculations for the $S = {}^3/_2$ model $[Fe(EDTA)NO]^{2-}$,[20] the spectrum of $Fe^{III}PCD\{NO^-\}$ could be assigned. No detectable broadening of the EPR resonance is observed when the $Fe^{III}PCD\{NO^-\}$ samples are prepared in ^{17}O-enriched water, indicating that the hydroxide bound to the resting ferric complex may no longer be present in the NO complex.[18] Also, since having two NO molecules bound would presumably lead to an $S = 1$ complex, the likely ligation for $Fe^{III}PCD\{NO^-\}$ is five-coordinate with two tyrosinates, two histidines, and one NO as shown in Figure 5A. In the energy region studied here (5000−28 000 cm^{-1}), only the tyrosinate and NO^- LMCT are expected to contribute to the observed transitions.[16] From the Gaussian fitting of the MCD and Abs spectra of $Fe^{III}PCD\{NO^-\}$, there are seven transitions in the range of 5000−28 000 cm^{-1}. Band 1 is assigned as the $^6A_1$ to $^4T_1$ transition and band 2 as the $^6A_1$ to $^4T_2$ ligand field transition. The intensity mechanism described in ref 18 indicates that in $\{FeNO\}^7$ complexes the spin-forbidden d → d transitions gain their intensity from coupling to NO^- *S*

(58) Orville, A. M.; Chen, V. C.; Kriauciunas, A.; Harpel, M. R.; Fox, B. G.; Münck, E.; Lipscomb, J. D. *Biochemistry* **1992**, *31*, 4602−4612.

(59) Solomon, E. I.; Hanson, M. A. Bioinorganic Spectroscopy. In *Inorganic Electronic Structure and Spectroscopy*; Solomon, E. I., Lever, A. B. P., Eds.; John Wiley & Sons: New York, 1999; Vol. II, pp 1−130.

$= 1$, which allows transitions from the $S_{TOT} = {}^3/_2$ ground state to the $S = {}^3/_2$ excited state, making them effectively spin-allowed and polarized along the Fe−NO bond.[20,57] Therefore, since band 1 is *xy*-polarized, the Fe−NO bond for Fe^{III}PCD{NO^-} is in the *xy*-plane of the ZFS coordinate system. Band 4 is very intense and also *xy*-polarized and is therefore assigned to be the NO^- op $2\pi^*$ to d_{yz} transition as in $[Fe(EDTA)NO]^{2-}$.[20] Band 3 is *z*-polarized and therefore a CT band associated with one of the two tyrosinates. The intensity and energy are comparable to LMCT transitions attributed to tyrosinate CT in PCD.[16] The remaining bands 5, 6, and 7 are CT from either the NO^- or the tyrosinates. The additional bands observed at 17 400 and 19 650 cm^{-1} in Figure 3 for the Fe−NO unit in $[Fe(EDTA)NO]^{2-}$ are not observed for Fe^{III}PCD{NO^-} and are likely masked by bands 1−3.

Comparing the transitions associated with the Fe−NO unit in PCD{NO} to those in $[Fe(EDTA)NO]^{2-}$ indicates three main differences. First, the energies of the d → d transitions are much higher, which is consistent with a decrease in coordination number since from the d^5 Tanabe−Sugano diagram lower ligand field strength leads to d → d transitions at higher energy.[60] Second, the main NO^- LMCT transition, NO^- op $2\pi^*$ to d_{yz} CT, is at nearly the same energy in both systems (≈1500 cm^{-1} lower in Fe^{III}PCD{NO^-}), indicating that the decrease in coordination number for Fe^{III}PCD{NO^-} is partially compensated by the strong donation of the other ligands. Third, the Fe−NO bond is no longer determining a strong *z*-direction as in $[Fe(EDTA)NO]^{2-}$ but rather the Fe−NO bond is in the *xy* plane, indicating a difference in bonding between the two complexes.

It is also interesting to note that while the MCD intensities of Fe^{III}PCD{NO^-} and $[Fe(EDTA)NO]^{2-}$ are comparable, the Abs intensity is much higher for Fe^{III}PCD{NO^-} (see ref 19 and Supporting Information), which is due to the presence of the additional intense low-energy tyrosinate to iron CT transitions in Fe^{III}PCD{NO^-}.

3. 3,4-PCD-PCA-NO. The low-temperature MCD spectrum for Fe^{III}PCD{PCA,NO^-} is shown in Figure 6A (solid lines). The RT Abs spectrum has a very pronounced λ_{max} at 24 500 cm^{-1} (see ref 19 and Supporting Information). The Gaussian resolution of the MCD data (dashed lines in Figure 6A) and the Abs data (not shown) indicate the presence of seven transitions in the 5000−28 000-cm^{-1} region.[57] The energies, $\nu_{1/2}$, Abs ϵ, MCD $\Delta\epsilon$, and f_{exp} are shown in Table 5. VTVH data were collected for Fe^{III}PCD{PCA,NO^-} for bands 1, 2, 3, 4, and 5. A *D*-value of +4 cm^{-1} was used for fitting Fe^{III}PCD{PCA,NO^-}, which was the midpoint of the range of +3−5 cm^{-1} obtained previously from EPR, and the *E/D* is 0.175.[21] The effective transition moments are given in Table 4. Bands 1 and 4 are fit as predominantly *z*-polarized transitions, while bands 2, 3, and 5 are predominantly *x*-polarized (Figure 6B−E). The rhombic *E/D* value signifies that the three principal directions of the *D*-tensor are inequivalent. The low value of *D* (3−5 cm^{-1}) indicates that

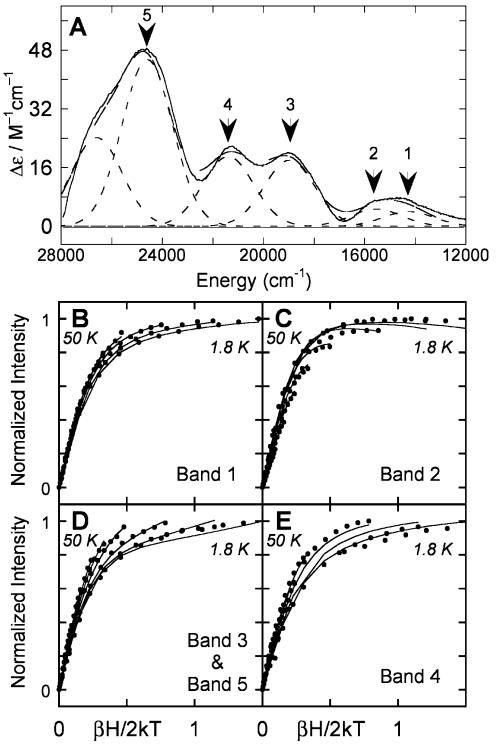

Figure 6. (A) Gaussian resolution (- - -) of Fe^{III}PCD{PCA,NO^-} MCD spectra (—) at 5 K and 7 T with arrows indicating at what energy the VTVH MCD data were taken. There are no MCD transitions between 5000 and 12 000 cm^{-1} and this region was omitted for clarity. Bottom: VTVH MCD data for Fe^{III}PCD{PCA,NO^-} collected between 0 and 7 T and between 1.6 and 50 K at (B) 14 100 cm^{-1} band 1, (C) 15 500 cm^{-1} band 2, (D) 19 100 cm^{-1} band 3, which is identical to 24 780 cm^{-1} band 5, and (E) 21 300 cm^{-1} band 4.

Table 5. Gaussian Resolution and Experimental Parameters for the Seven Observed Transitions of Fe^{III}PCD{PCA,NO^-}

band	Abs energy (cm^{-1})	ϵ (mM^{-1} cm^{-1})	Abs $\nu_{1/2}$ (cm^{-1})	f_{exp}	MCD energy (cm^{-1})	$\Delta\epsilon$ (M^{-1} cm^{-1})	MCD $\nu_{1/2}$ (cm^{-1})
1	14 270	0.310	3770	0.005	14 270	3.7	2354
2	15 690	0.400	3770	0.007	15 550	4.3	2354
3	18 980	0.400	3770	0.007	18 980	17.6	2354
4	21 400	1.80	3770	0.03	21 400	18.8	2354
5	24 600	3.40	3770	0.06	24 600	45.5	2354
6	26 600	0.700	3770	0.01	26 600	23.4	2354
7	29 000	3.00	3770	0.05			

the ZFS of Fe(III) is greatly reduced since the *D* of {FeNO}^{7} systems originates from the vector coupling of *D* of the Fe(III) with that of the NO^- $S = 1$ and the coupling coefficient of the Fe(III) into the $S = {}^3/_2$ ground state are much higher (28/15 * *D*-tensor of the ferric center vs 1/15 * NO^- $S = 1$ *D*-tensor).[61]

These polarizations greatly aid in the assignment of the Abs/MCD spectrum. XAS pre-edge and EXAFS data together indicate that Fe^{III}PCD{PCA,NO^-} is likely a highly distorted six-coordinate site, which is consistent with the increased MCD energies of the d → d transitions (vide infra). For Fe^{III}PCD{PCA,NO^-} EPR hyperfine broadening is observed when the C4 but not the C3 hydroxyl group is labeled with ^{17}O, indicating that the substrate may have weak hyperfine coupling along one axis due to a long bond.[18] A

(60) Sugano, S.; Tanabe, Y.; Kamimura, H. *Multiplets of Transition-Metal Ions in Crystals*; Academic Press: New York, 1970.

(61) Kahn, O. *Molecular Magnetism*; VCH Publishers: New York, 1993.

structure consistent with these findings for Fe^{III}PCD{PCA,NO^-} and with previous spectroscopic and crystallographic results[22] is shown in Figure 5B. The catecholate can either be a protonated monoanion or a dianion, where in the latter, ketonization will also lead to a long bond. In addition to the tyrosinate and NO^- LMCT transitions observed for Fe^{III}PCD{NO^-}, CT transitions for Fe^{III}PCD{PCA,NO^-} are now also expected from the catecholate ligand. Gaussian fitting of the MCD and Abs spectra of Fe^{III}PCD{PCA,NO^-} indicates that there are seven transitions in the region of 5000−35 000 cm^{-1}. In Fe^{III}PCD{PCA} there is a new low-energy transition from the substrate.[8,35,62] By analogy, band 1 in Fe^{III}PCD{PCA,NO^-} is assigned as the substrate to Fe(III) CT transition and it is *z*-polarized. Band 4, which is also *z*-polarized, may be a substrate CT transition as well. Alternatively, it could be attributed to the tyrosinate trans to the substrate. The Fe−NO bond would be orthogonal to the substrate−Fe(III) bond as shown in Figure 5B and therefore the *x*-polarized bands 2, 3, and 5 can be attributed to the NO^- ligand. Band 2 contains the two d → d transitions (which cannot be resolved) while band 5 is the intense NO^- $2\pi^*$ to d_{yz} transition by analogy to $[Fe(EDTA)NO]^{2-}$ and Fe^{III}PCD{NO^-}. Band 3 contains the NO^- ip to d_{xz} and NO^- ip to $d_{x^2-y^2}$ CT transitions. Band 6 is likely due to tyrosinate or substrate CT.

A number of interesting points arise from the MCD data for Fe^{III}PCD{PCA,NO^-}. First, as in Fe^{III}PCD{NO^-}, the NO ligand does not define the dominant *z*-direction. In fact, from the EPR data, Fe^{III}PCD{PCA,NO^-} has no single strong direction and is quite rhombic ($E/D = 0.175$). This is consistent with the XAS pre-edge and EXAFS analyses. The pre-edge lacks the additional intensity commonly seen upon NO binding to iron, and the lack of a short Fe−NO bond from EXAFS precludes the possibility of a single strong (i.e., axial) direction. Second, the energy of the dominant Fe−NO band is higher by >2000 cm^{-1} than for both Fe^{III}PCD{NO^-} and $[Fe(EDTA)NO]^{2-}$, reflecting the stronger donation from the catecholate ligand, which shifts the d-manifold to higher energy. Third, the energies of the d → d transitions are consistent with the six-coordinate site implied from EXAFS fits. Finally, the larger splitting of the NO^- op to d_{yz} and NO^- ip to $d_{x^2-y^2}$ and d_{xz} CT transitions relative to $[Fe(EDTA)NO]^{2-}$ reflects the difference in the Fe−NO geometry since the splitting of the π_{ip} and π_{op} NO^- orbitals is due to the bending of the Fe−NO unit. As the Fe−N−O angle decreases the bonding changes from solely π-bonding from the ip and op NO orbitals to π-bonding plus pseudo-σ bonding as depicted in Scheme 2 where upon bending the ip NO orbital bonding changes from π to σ. The Fe−NO angle of the EDTA complex is 156°.[20] An increase in the splitting of the NO^- ip and op orbitals is consistent with the decrease in Fe−NO angle for Fe^{III}PCD{PCA,NO^-} (<150°) from the EXAFS analysis.

Discussion

The combination of XAS, Abs, MCD, VTVH MCD, and EPR was used here to develop an understanding of the NO binding to the iron site in Fe^{III}PCD{NO^-} and Fe^{III}PCD{PCA,NO^-} relative to other {FeNO}^{7} complexes. The pre-edge intensities of Fe^{III}PCD{NO^-} and Fe^{III}PCD{PCA,NO^-} do not show the increased intensity upon NO binding typical of {FeNO}^{7} model complexes with strong Fe−NO bonds and the VTVH MCD data show that the NO to Fe CT is no longer polarized along the *z*-axis of the ZFS tensor. The EXAFS determined Fe−NO bond lengths in Fe^{III}PCD{NO^-} and Fe^{III}PCD{PCA,NO^-} are unusually long for {FeNO}^{7} complexes and correlate with the modified transition intensities, polarizations, and energies in MCD and Abs spectra. All of the transitions observed arise from either d → d transitions or NO^-, tyrosinate, or PCA LMCT transitions and can be used to gain insight into the coordination number and bonding of these ligands, particularly NO^-, to the metal site.

Scheme 2. Fe−NO Bonding

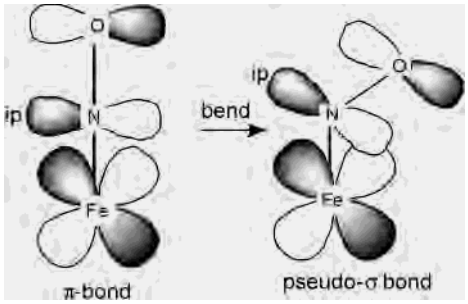

Effect of Donor Strength on NO Bonding. From XAS edges, the {FeNO}^{7} unit clearly involves CT to produce an active site with formal oxidation states of Fe(III) and NO^-.[20,63] Two main electronic configurations have been proposed that could lead to an $S = {}^3/_2$ {FeNO}^{7} system.[20,23,26,64] The iron could be a high-spin ferric center, which is antiferromagnetically coupled to an $S = 1$ NO^- ligand,[20,23] or the binding of the strong NO donor could lead to an intermediate $S = {}^3/_2$ state on the Fe(III) bound to an $S = 0$ NO^- ligand.[64] In the protein system studied here, the significantly longer and weaker Fe−NO bond compared to that in other $S = {}^3/_2$ systems precludes the possibility of an intermediate spin ferric center, yet the net spin of the system is still $S = {}^3/_2$. This supports earlier results[20,23] which indicated that the $S = {}^3/_2$ system in mononuclear non-heme iron model complexes and proteins is best described as high-spin Fe(III) $S = {}^5/_2$ center antiferromagnetically coupled to an NO^- $S = 1$ ligand.

The strength of the Fe−NO bonds for Fe^{III}PCD{NO^-} and Fe^{III}PCD{PCA,NO^-} can be compared to other {FeNO}^{7} $S = {}^3/_2$ complexes such as $[Fe(EDTA)NO]^{2-}$. The Fe−NO bonding of this model complex is quite different from that in the enzyme species, as can be seen from VTVH MCD, XAS pre-edge, and EXAFS spectroscopies. EXAFS data show that the bond length of the Fe−NO unit is 1.74 Å for $[Fe(EDTA)NO]^{2-}$ but has increased significantly to ≥1.91 Å in the PCD complexes.[20] Furthermore, the lack of a

(62) Bull, C.; Ballou, D. P. *J. Biol. Chem.* **1981**, *256*, 12673−12680.

(63) Westre, T. E., Ph.D. Thesis. Department of Chemistry, Stanford University, Stanford, CA, 1995.

(64) Enemark, J. H.; Feltham, R. D. *Coord. Chem. Rev.* **1974**, *13*, 339−406.

multiple-scattering wave in the EXAFS fits indicates an abnormally bent Fe−NO unit in the protein systems studied here. For $[Fe(EDTA)NO]^{2-}$ the unique strong interaction at the iron is due to the Fe−NO bond as indicated by the fact that all of the Fe−NO CT transitions in VTVH MCD are *z*-polarized. The short Fe−NO bond defines the *z*-axis of the ZFS tensor and the NO^- to Fe(III) CT transitions are all polarized along this bond. In contrast, for both $Fe^{III}PCD\{NO^-\}$ and $Fe^{III}PCD\{PCA,NO^-\}$ the Fe−NO transitions are no longer *z*-polarized, indicating that the Fe−NO bond no longer defines the unique strong bonding direction. This is further illustrated by the fact that the pre-edges of the $Fe^{III}PCD\{NO^-\}$ and $Fe^{III}PCD\{PCA,NO^-\}$ complexes do not show a large increase in intensity typical of model $\{FeNO\}^7$ systems with short, strong Fe−NO bonds. Thus, the electronic and geometric structure of the $\{FeNO\}^7$ unit in the $Fe^{III}PCD\{NO^-\}$ and $Fe^{III}PCD\{PCA,NO^-\}$ complexes are quantitatively distinct from $[Fe(EDTA)NO]^{2-}$ and other model complexes where the Fe−NO bond is short and strong and defines the *z*-axis of the ZFS tensor.

The weaker Fe−NO binding for $Fe^{III}PCD\{NO^-\}$ and $Fe^{III}PCD\{PCA,NO^-\}$ can, at least in part, be attributed to the other donor ligands in $Fe^{III}PCD\{\}$ and $Fe^{III}PCD\{PCA\}$, which are unusually strong relative to the EDTA ligand in the $[Fe(EDTA)NO]^{2-}$ complex. This can be seen from the Abs, MCD, and XAS spectroscopic results. From the electronic spectra of the three species, $[Fe(EDTA)NO]^{2-}$ has significantly lower total absorption intensity as compared to $Fe^{III}PCD\{NO^-\}$ and $Fe^{III}PCD\{PCA,NO^-\}$. This is due to the intense low-energy ligand to metal CT transitions in $Fe^{III}PCD\{NO^-\}$ and $Fe^{III}PCD\{PCA,NO^-\}$ that have been shown to arise from both tyrosinate and catecholate ligands.[8,16,62,65] These intense, low-energy CT transitions indicate highly covalent interactions between these ligands and the Fe(III) center in the protein. The XAS edge energy also reflects this increase in donor strength since the edge shifts to lower energy (more charge donation) across the series: $[Fe(EDTA)NO]^{2-}$ > $Fe^{III}PCD\{\}$ > $Fe^{III}PCD\{NO^-\}$ > $Fe^{III}PCD\{PCA,NO^-\}$ and $Fe^{II}PCD\{\}$. The increased charge donation from the endogenous tyrosinate and from the substrate ligands stabilizes the ferric ion and reduces the donor interaction of NO^- with the Fe^{III}, weakening the bond.

The Fe−NO bond in $Fe^{III}PCD\{NO^-\}$ and $Fe^{III}PCD\{PCA,NO^-\}$ may also be impacted by the hydrogen bond interactions in the active site pocket. The crystal structures of $Fe^{III}PCD\{INO,CN^-\}$ and $Fe^{III}PCD\{NNO,CN^-\}$ show a hydrogen bond interaction between the CN nitrogen and the amide of Y16 (Scheme 3).[10] The effect of the hydrogen bond on a negatively charged NO^- ligand binding in this position could also stabilize the NO^- and weaken the Fe−NO bond. It should be noted, however, that $[Fe(EDTA)NO]^{2-}$, which does not have strong donor ligands but is in a strong hydrogen-bonding glycerol−water solvent, is found from EXAFS to have a short Fe−NO bond.[24] In the PCD system, the hydrogen bonding can contribute to the binding energy of the NO^- to the protein pocket and play a role in its competition with substrate for binding to the site.

Scheme 3. Crystal Structure of the Active Site of $Fe^{III}PCD\{INO,CN^-\}$ (Ref 11) Exhibiting a Hydrogen Bond between the CN^- and the Amide of Y16 (- - -)[a]

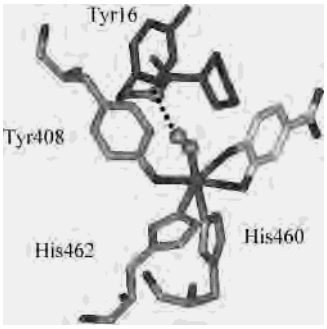

[a] Note that for clarity the orientation of the active site is different in this scheme relative to that of Scheme 1. Copyright 1997 American Chemical Society.

Functional Significance. The EXAFS determined Fe−NO bond length for the extradiol dioxygenase catechol 2,3-dioxygenase (2,3-CTD) with catechol and NO bound is significantly shorter than the Fe−NO bond (1.74 vs ≈1.96 Å) length obtained for the $Fe^{III}PCD\{PCA,NO^-\}$ complex studied here.[65] On the basis of the crystal structures of the enzyme−substrate complexes for both the intra- and extradiol dioxygenases, their enzyme−substrate−NO complexes should be congruent, with the major difference being the substitution of the equatorial tyrosinate ligand of the intradiol dioxygenases for a monodentate glutamate in the extradiol dioxygenases.[10,66,67] This allows a direct comparison of the iron−substrate interactions at the same oxidation state and may provide insight into the different reactivities. There is also a difference in hydrogen bonding to the NO, where in contrast to PCD, the proposed O_2 binding site in the extradiol is principally hydrophobic and lacks hydrogen bond donors in the vicinity of the NO molecule. The increased tyrosinate donation stabilizes the oxidized site relative to the reduced site in the intradiol dioxygenases, resulting in a low reduction potential and a catalytically relevant ferric site. This favors a mechanism of substrate activation by Fe(III) of intradiol enzymes over the mechanism of charge donation to give Fe(II), which reacts directly with O_2 as proposed for extradiol cleaving enzymes.[3,68]

A crystal structure of another member of the mononuclear non-heme iron group of enzymes, IPNS, has been solved with both the substrate and NO bound to the iron center.[32] The system is also described as an $S = {}^3/_2$ system from EPR.[58,69] Interestingly, while the ligands for the free enzyme are similar to those of the extradiol dioxygenases (i.e., both have the two histidine-one carboxylate facial triad[70] and two waters as ligands, with IPNS having an additional glutamine

(65) Shu, L.; Chiou, Y.-M.; Orville, A. M.; Miller, M. A.; Lipscomb, J. D.; Que, L., Jr. *Biochemistry* **1995**, *34*, 6649−6659.

(66) Bolin, J. Personal communication.
(67) Senda, T.; Sugiyama, K.; Narita, H.; Yamamoto, T.; Kimbara, K.; Fukuda, M.; Sato, M.; Yano, K.; Mitsui, Y. *J. Mol. Biol.* **1996**, *255*, 735−752.
(68) Funabiki, T.; Yamazaki, T. *J. Mol. Catal. A* **1999**, *120*, 37−47.
(69) Chen, V. J.; Orville, A. M.; Harpel, M. R.; Frolik, C. A.; Surerus, K. K.; Münck, E.; Lipscomb, J. D. *J. Biol. Chem.* **1989**, *264*, 21677−21681.
(70) Hegg, E. L.; Que, L., Jr. *Eur. J. Biochem.* **1997**, *250*, 625−629.

as the sixth ligand)[70] the ACV substrate is a very strong thiolate donor.[32,71] From the high-resolution (1.45 Å) structure, the Fe−NO bond is unusually long (2.13 Å) compared to that in the other systems (i.e., $[Fe(EDTA)NO]^{2-}$ and the catechol 2,3-dioxygenase−catechol−NO complex) but similar to that in the PCD protein system studied here.[20,32,65] Unlike in $Fe^{III}PCD\{NO^-\}$ and $Fe^{III}PCD\{PCA,NO^-\}$, the strong donor ligand is only present when the substrate binds to the Fe(II) center in the catalytic mechanism of IPNS. The additional strong thiolate ligand would decrease the interaction of iron with donor ligands (i.e., a water comes off) and increase its reaction with acceptor ligands such as O_2. Additionally, the strong charge donation of the thiolate to the resulting $Fe^{III}-O_2^-$ putative intermediate could activate its β-methylene hydrogen for abstraction by the superoxide.[57]

Summary

In summary, XAS, Abs, MCD, VTVH MCD, and EPR spectroscopies have been used to probe the $\{FeNO\}^7$ bond in $Fe^{III}PCD\{NO^-\}$ and $Fe^{III}PCD\{PCA,NO^-\}$. As deduced from the EXAFS bond lengths, this bond is much weaker than that in model systems. This is also observed from the low pre-edge intensity and the change in polarization of the Fe−NO LMCT transitions relative to the ZFS tensor. This directly reflects the increased donor strength of the other ligands (tyrosinate and PCA) and shows that their coordination can greatly affect reactivity. In intradiol dioxygenases the endogenous tyrosinate ligands stabilize the catalytically relevant Fe(III) state. This is in contrast to IPNS, for which binding of the strongly donating thiolate of the substrate ACV to Fe^{II} leads to water loss (creating a binding site for O_2), and provides increased electron density to stabilize the $Fe-O_2$ bond, thereby increasing the reactivity of the Fe(II) center with O_2.

Acknowledgment. This research was supported by NIH grant GM40392 (E.I.S.), NIH Grant GM24689 (J.D.L.), and NIH Grant RR01209 (K.O.H.). M.I.D. thanks the Evelyn Laing McBain Fund for a doctoral fellowship. J.M.Z. thanks the Jane Coffin Childs Fund for Medical Research for a postdoctoral fellowship. SSRL is funded by the Department of Energy, Office of Basic Energy Sciences. The SSRL Structural Molecular Biology program is funded by the National Institutes of Health, National Center for Research Resources, Biomedical Technology Program, and the Department of Energy, Office of Biological and Environmental Research.

Supporting Information Available: UV−visible absorption spectra of $[Fe(EDTA)NO]^{2-}$, $Fe^{III}PCD\{NO^-\}$, and $Fe^{III}PCD\{PCA,NO^-\}$. This material is available free of charge via the Internet at http://pubs.acs.org.

IC025906F

(71) Han, S.; Eltis, L. D.; Timmis, K. N.; Muchmore, S. W.; Bolin, J. T. *Science* **1995**, *270*, 976−980.